Article

Effect of Humidity on Interfacial Debonding Behavior Between Larger Graphene Sheet and Cement-Based Composites

Yongliang Han [1,2,*], Yongzhe Zhao [2], Yijie Wang [2] and Tong Chen [3]

[1] CCTEG Xian Research Institut (Group) Co., Ltd., Xi'an 710077, China
[2] CCTEG Xi'an Geothermal Energy Development Co., Ltd., Xi'an 712100, China;
zhaoyongzhe@cctegxian.com (Y.Z.); 13109506418@163.com (Y.W.)
[3] Shaanxi Coal Industry Fengjing New Energy Technology Co., Ltd., Xi'an 710300, China; 15191462423@163.com
[*] Correspondence: yaqingyxgs1885@163.com

Abstract: This paper investigates the interface debonding behavior of graphene (G) on a calcium silicate hydrate (C-S-H) substrate using molecular dynamics (MD) simulations. The effect of interfacial water content on the debonding behavior of graphene on cement-based composites was studied. Simulation results reveal that there is only a van der Waals force between G and C-S-H; the interface bonding strength is weak; and the debonding properties (maximum peeling force (F_{max}) and work (W)) are low. The debonding energy of graphene decreases with an increase in interfacial water content, indicating that water intrusion will weaken the binding effect of G and C-S-H, and reduce the difficulty of graphene's debonding on a C-S-H substrate. Exploring the adhesion behavior of graphene on C-S-H under the influence of humidity at the nanoscale is of great significance for understanding the basic adhesion mechanism, optimizing composite material properties, and promoting the development of related disciplines.

Keywords: molecular dynamics simulation; graphene; calcium silicate hydrate; interfacial debonding properties

1. Introduction

Graphene (G) is a new type of carbon nanomaterial discovered in recent years. As a unique single-layer two-dimensional material, graphene has many excellent properties. For a large specific surface area, the theoretical value can reach 2600 m^2/g [1]. It has excellent mechanical properties, a tensile strength of 125 GPa, and an elastic modulus of up to 1.1 TPa [2]; its strength is about 100 times that of ordinary steel. With excellent thermal conductivity, the thermal conductivity of single-layer graphene can reach 5300 W/mK, which is higher than the 3500 W/mK of ordinary carbon nanotubes [3,4]. With excellent electrical properties, graphene has surprisingly high electron mobility, with a resistivity of 10^{-6} Ω·cm, which is slightly less than that of silver that is 10^{-6} Ω·cm [5,6]. At present, graphene materials have shown great application potential in many fields, such as electronics, biomedicine, and energy storage, and have also attracted much attention in the field of cement-based materials [7,8].

Calcium silicate hydrate (C-S-H) gel is the main product of cement hydration and the main component that provides the bonding strength of cementing materials, which determines the mechanical and durability properties of cement materials [9,10]. G and C-S-H gel interact together to form a sandwich-like composite structure, which significantly improves the mechanical properties of cement-based materials [11]. However, under external loads (shear, tensile, torsion, etc.), the interface of the composite structure may be subject to graphene-based material debonding and other phenomena. This debonding behavior causes the graphene-based material adsorbed on the C-S-H gel substrate to lose its strengthening effect, which directly affects the properties of the composite structure [12,13]. In addition, cement-based materials, as an important component of infrastructure such

as water conservancy projects, are often subjected to external water intrusion, which will affect the performance of the graphene/C-S-H interface interaction, and then affect the working performance of modified cement-based composites.

Humidity has a significant impact on the adhesion behavior of graphene on C-S-H [14]. Under dry conditions, the adhesion between graphene and C-S-H mainly relies on physical interactions such as van der Waals forces [15], which, although stable, may be weakened in humid environments [16]. When environmental humidity increases, the intervention of water molecules will change the charge distribution and polarity of graphene and C-S-H surfaces, thereby affecting the interaction force between the two [17]. On the one hand, water molecules have polarity and can adsorb on the surfaces of graphene and C-S-H, forming a thin water film. This water film may weaken direct physical contact between graphene and C-S-H, leading to a decrease in adhesion. On the other hand, if there are hydrophilic functional groups on the surface of graphene or C-S-H, water molecules can also act as bridges to promote binding between graphene and C-S-H through interactions such as hydrogen bonding [18]. This strengthening effect is usually not as strong as direct chemical bonding.

However, it is worth noting that the effect of humidity on the adhesion behavior of graphene on C-S-H is not always negative. In some cases, moderate humidity can promote chemical reactions between graphene and C-S-H [19], such as accelerating hydrolysis or ion exchange processes, thus facilitating the formation of stronger chemical bonds. In addition, water molecules may also participate in the oxidation process of the graphene surface [20], indirectly increasing the number of active functional groups on its surface, thereby enhancing its adhesion ability with C-S-H.

At present, it is difficult to analyze the mechanism of water molecules on the G/C-S-H interface at a nanoscale. A molecular dynamics (MD) method is usually used for research [21,22]. Scholars have successfully studied the thermal and mechanical properties of interfaces. An interaction model between foam asphalt and aggregate was constructed, and the effects of factors such as the water content of foam asphalt, aggregate type, aggregate surface moisture, and temperature on interfacial adhesion between foam asphalt and aggregate were analyzed through molecular dynamics simulations [23]. Additionally, molecular dynamics simulations were employed to investigate the interfacial bonding properties between carbon fibers and epoxy resin, particularly focusing on the influence of water molecules on these properties [24]. Regarding the issue of oil–water interfacial adhesion, molecular dynamics simulations were utilized to study the arrangement and orientation of water molecules at the oil–water interface, as well as the factors influencing oil–water interfacial adhesion [25]. Through molecular dynamics simulations, the behavior of water molecules on different solid surfaces (such as hydrophilic and hydrophobic surfaces) was observed, along with the impact of these behaviors on the wettability of solid surfaces [26]. By using MD, the essence of humidity on G/C-S-H interface interaction forces, such as van der Waals forces, hydrogen bonds, ionic bonds, etc., can be revealed, as well as how they collectively affect adhesion strength between G and C-S-H. This is crucial for understanding the overall performance of composite materials, optimizing adhesion between G and C-S-H, and ensuring the stability and durability of composite materials.

Therefore, in this study, MD simulation [27] technology was used to study the debonding behavior of G on a C-S-H gel surface at different water contents at a nanoscale, and the interface bonding strength was evaluated during the debonding simulation. The mechanism of the influence of water on the debonding behavior of G on a C-S-H substrate was revealed.

2. Model and Methodology

2.1. Model

In this study, the graphene model is derived from graphite crystals as shown in Figure 1a. Considering computational efficiency and referring to relevant studies, the paper sets the wafer size to about 8 nm. For this scale, flatness will not cause some areas of the

sheet to detach from the substrate surface. But for larger sizes, the effect of flatness needs to be considered [28]. Construction of the C-S-H gel model was mainly based on the studies of Pellenq et al. [29], and tobermorite 11 Å crystal was used as the initial configuration. After deleting all the water molecules in the model, a $4 \times 3 \times 1$ supercell was constructed, and neutral silica groups in the supercell were randomly deleted to achieve the target Ca/Si ratio of 1.7 [30]. The final model contains 144 calcium atoms, 85 silicon atoms, and 311 oxygen atoms. At this time, the density of the model is 1.94 g/cm^3; the distribution of polymerization degree Q is: $Q_0 = 1.2\%$, $Q_1 = 63.5\%$, $Q_2 = 35.3\%$; and the average length of the silicon chain is 3.1. Subsequently, the Monte Carlo (GCMC) method was used to adsorb water molecules with a density of 1.00 g/cm^3 into the dry C-S-H gel model as shown in Figure 1b. After adsorption, the density of the C-S-H gel model was 2.33 g/cm^3. The chemical formula of the C-S-H gel obtained by the above method is $(CaO)_{1.7}(SiO_2)(H_2O)_{1.75}$. By stretching the C-S-H model, a relatively stable interface structure containing interlayer calcium was obtained. The surface of the orthogonal structure breaks and exposes interlayer calcium ions and non-bridging oxygen atoms. For closing to the real gel surface, the protonation of Si–O$^-$ on the surface of the structure forms Si–OH.
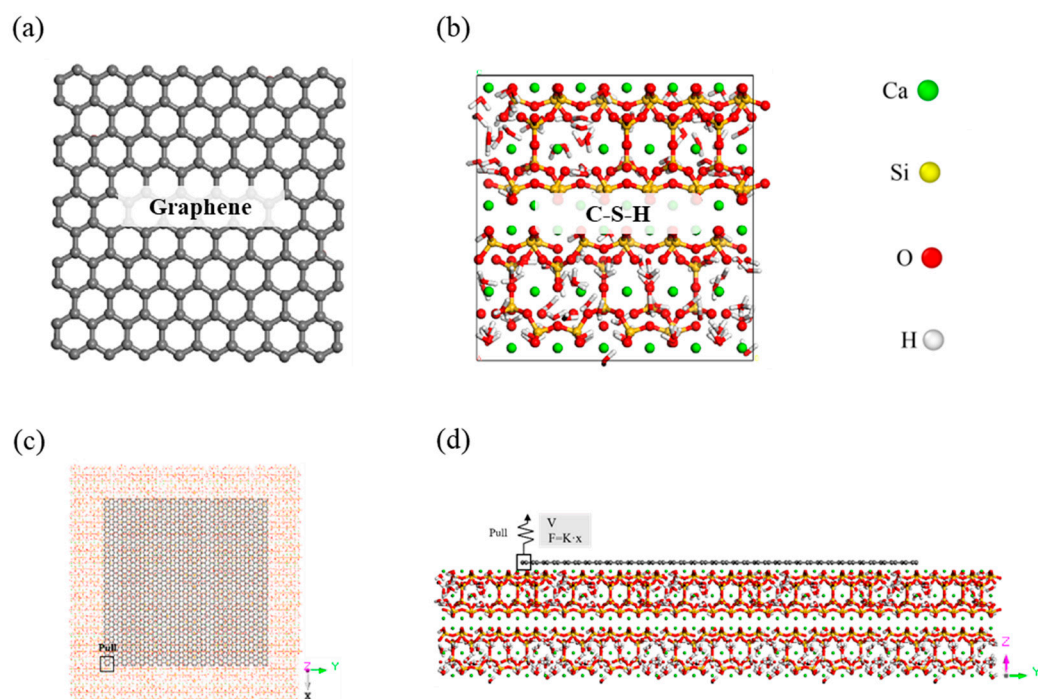
Figure 1. Atomic structures of (**a**) the graphene sheet, (**b**) C-S-H gel model, (**c**) debonding model—top view, and (**d**) debonding model—front view.

2.2. Force Field

The force fields used in this study are ClayFF (Clay Force Field) by Cygan et al. [31] and OPLS-AA (Optimized Potentials for Liquid Simulations) [32]. The ClayFF force field is suitable for the simulation of aqueous and multi-component mineral systems and their interfaces with aqueous solutions [33], and the OPLS-AA force field was developed by Jorgensen's team, both of which are widely used for molecular dynamics simulation of the thermal and mechanical properties of C-S-H and G/graphene oxide [34–36].

2.3. Simulation Process

The molecular dynamics simulation in this study was performed using the LAMMPS (version lammps-8Apr2021) software package [37]. At present, some experiments have been conducted on the adhesion of composite nanomaterials from a macro perspective, but the lack of analysis on the mechanism at the atomic level is urged to be solved. Using LAMMPS software, researchers studied interfacial behavior from the perspective of the essential

properties of nanomaterials, and analyzed the thermodynamics of nano-adsorption. A vacuum layer in the z-axes with periodic boundary conditions on the x- and y-axes is set (in Figure 1d). G is placed flat on the C-S-H interface, and water molecules are located between G and C-S-H as discussed in Section 3.3. After the model is determined, the energy is minimized by a conjugate gradient method to ensure rationality of the structure in the calculation process. At the relaxation stage, the model is relaxed to 100 ps in the NVT ensemble at room temperature (300 K). After relaxation, the debonding behavior and mechanical response of G at the C-S-H interface were studied in the NVT ensemble. The spring connects the middle part of graphene to eliminate the influence of tangential force when G peels off on C-S-H. During the peeling process, graphene always experiences the highest force in the middle to obtain the maximum peeling force. During the tensile testing process, the distribution of stress on the graphite layer is uniform as the tension caused by elastic deformation of the spring is uniformly transmitted to the graphite layer through the contact area. During the simulation, the carbon atom in the lower left corner of the G is selected as the position where the tension is applied (Figure 1a,b). Among them, the C-S-H matrix is fixed, and the external force is applied by virtual spring force based on Hooke's law. The schematic diagram of peeling is shown in Figure 2. By applying vertical drawing speed to the upper sheet, the tension and work information of the graphene-based sheet on C-S-H are obtained. In order to avoid deformation of the graphene-based sheet structure caused by a too-fast drawing speed, the spring elastic coefficient was set to 1000 pN/Å and the constant speed was set to 0.00001 Å/fs. A higher elastic stiffness can ensure accuracy of the simulation and avoid the impact of oscillation caused by the virtual spring effect on the peeling process [38]. The output average is sampled every 10,000 steps to minimize system error. In the whole process, the time step is set to 1 fs. 10 times steered MD trajectories are sampled to improve the accuracy of the calculation.
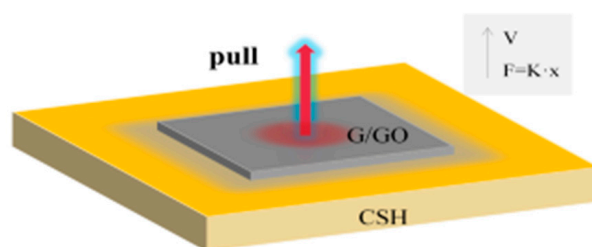
Figure 2. Schematic diagram of detachment model of G on C-S-H substrate. The yellow area is the C-S-H substrate, the gray area is the graphene layer, and the stress area is indicated by the red arrow.

3. Results and Discussion

3.1. Interface Structure of G and C-S-H

The properties of materials depend on their own structural characteristics, so the atomic density distribution inside G and C-S-H composites in the z direction was analyzed as shown in Figure 1a. c represents carbon atoms in G, and cah, cao, si, obos, ob, ow, and hw represent interlayer calcium ions, intra layer calcium ions, silicon atoms, unbridged oxygen atoms, bridged oxygen atoms, oxygen atoms in water, and hydrogen atoms in water, respectively, in C-S-H. The shaded part of the graph is the distribution (Figure 3a) of graphene carbon atoms in the z direction, which can reflect the degree of deformation of G. The results show that the height of the G distribution region in the z direction is about 3.20 Å, and there is no direct contact with the surface of C-S-H, indicating that C-S-H has a small adsorption effect on G, and the degree of structural deformation of G is small, which can also be reflected in Figure 3b because there is only a van der Waals force between G and C-S-H. The combination of the two is weak.
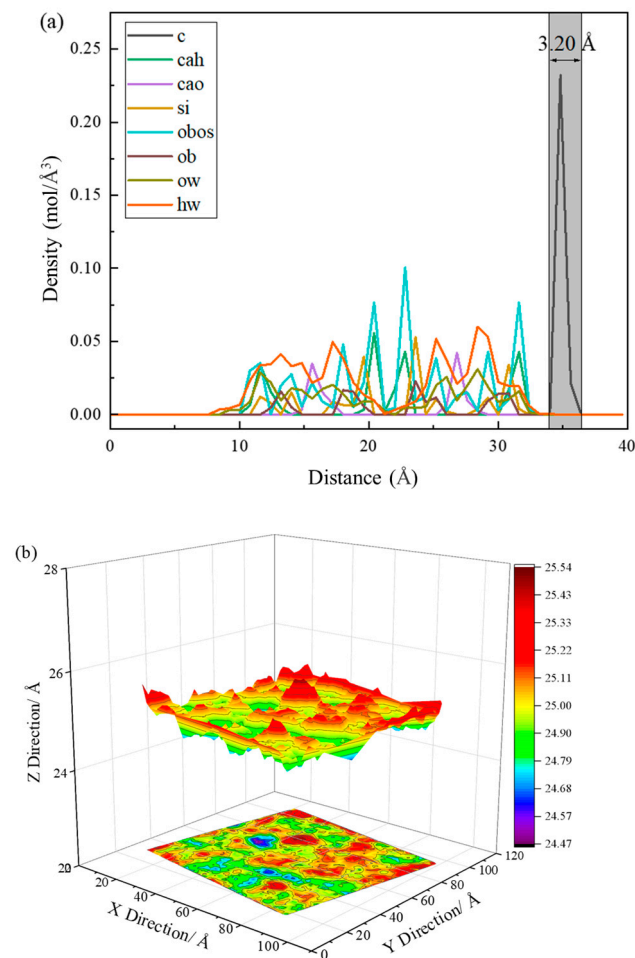
Figure 3. (**a**) Atomic density distribution of G and C-S-H composites along the z direction, (**b**) G interface structure.

3.2. Debonding Process and Debonding Properties of G on C-S-H

Figure 4a shows the dynamic debonding process of G on a C-S-H substrate, where a, b, c, and d are simulated snapshots of 0 ps, 2000 ps, 5000 ps, and 10,000 ps, respectively. The simulation results show that G can debond stably on a C-S-H substrate under the action of external forces, and some discontinuous folds and ripples appear in the process of debonding. In order to quantitatively demonstrate the debonding process, the time evolution of tension F and tension work W was recorded as shown in Figure 4. Tensile force can be regarded as feedback of the interaction between the G sheet and C-S-H, and is directly related to interfacial stress transfer. Tensile force acts on G, causing G to debond on the C-S-H substrate, and the tensile force performs work on it during the debonding process. Therefore, the debonding force F and the debonding work W can be used to characterize the debonding energy of G. The tension curve increases at first and then decreases with time, reaching a maximum $F_{max} = 1.42 \times 10^3$ pN at 5000 ps, and the work curve increases rapidly at first and then slowly and finally tends to be horizontal, reaching a maximum $W_{max} = 989.50$ Kcal/mol at about 9000 ps. The maximum debonding force F_{max} occurs at the moment when G is debonding at C-S-H, indicating the largest force barrier that G needs to overcome for debonding. The final work W_{max} appears when G is completely debonding on the C-S-H substrate, indicating the external energy required for complete debonding of G. Therefore, in this study, we mainly discussed the debonding behavior of G on a C-S-H substrate from the above two indicators.
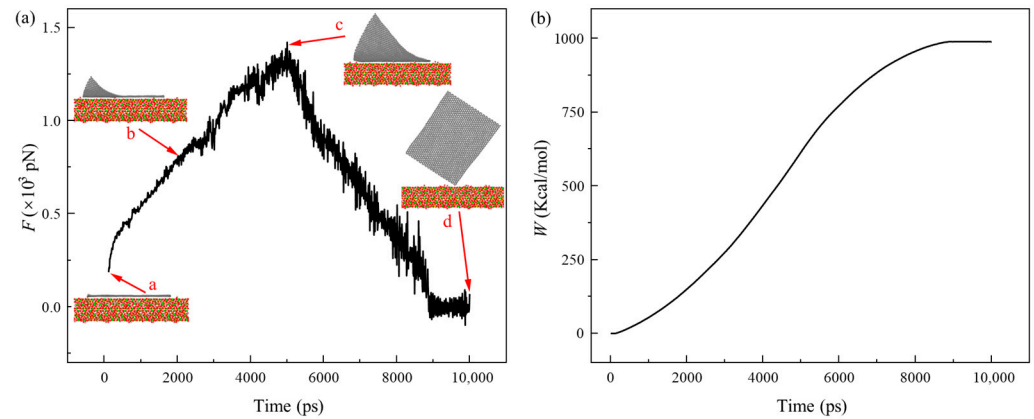
Figure 4. (**a**) Change of *F* with time, (**b**) change of *W* with time. Gray is graphene, which undergoes the following four processes on a CSH substrate, a: flat spreading, b: slow peeling of the plane, c: edge peeling, and d: complete peeling.

The debonding of G on a C-S-H substrate depends on the binding effect of C-S-H and G; the stronger the binding effect, the higher the difficulty of G on a C-S-H substrate, and the stronger its debonding ability. Potential energy (Pe) is energy stored in a system that can be released or converted into other forms of energy when the system is deformed. Figure 5a shows the change of system potential energy with time in the process of G debonding. The results show that the system potential energy in the process of debonding presents a slightly increasing trend with time, which is the result of work performed by external forces. The increased potential energy reflects the bonding strength provided by G when interacting with the C-S-H substrate.
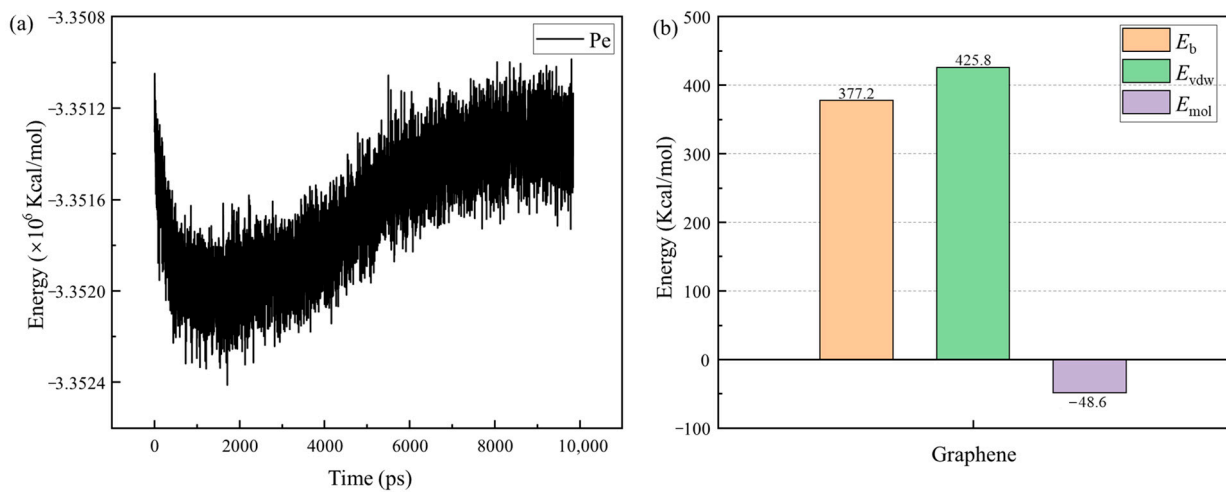
Figure 5. (**a**) Change of potential energy with time, (**b**) binding energy and binding energy decomposition of G/C-S-H.

Binding energy (E_b) refers to the energy released when two materials are combined into a whole from a free state. The greater the binding energy, the higher the stability of the structure, the stronger the adsorption effect of C-S-H on the graphene group, and the more external energy is required to overcome the binding energy to make graphene debond on the C-S-H substrate. Eb can be expressed as follows:

$$E_b = E_{total} - (E_{surface} + E_{c\text{-}s\text{-}h}) \tag{1}$$

where, E_{total} is the total potential energy of the C-S-H/G system; $E_{surface}$ is the potential energy of G; and $E_{c\text{-}s\text{-}h}$ is the potential energy of C-S-H. Figure 5b shows the binding energy of G with a binding energy of 377.2 Kcal/mol. For binding energy, energy decomposition

analysis is performed to determine the terms that play a major role in interfacial adhesion. Binding energy can also be expressed as [15] follows:

$$E_{\text{b}} = \Delta E_{\text{pair}} + \Delta E_{\text{mol}} \tag{2}$$

In the formula, ΔE_{pair} is a non-bond interaction, including a hydrogen bond, van der Waals force, and electrostatic coulomb interaction. This is mainly the van der Waals effect, which is 428.5 Kcal/mol. And ΔE_{mol} is a bond interaction formed by covalent bonds between atoms, including stretching, bending, and torsion, and is −48.6 Kcal/mol. Figure 5b shows the energy decomposition of the binding energy between G and the substrate C-S-H. The results show that the relationship between the two energies is $E_{\text{pair}} > E_{\text{mol}}$ in which only the van der Waals force exists in the non-interaction between G and C-S-H, indicating that the van der Waals force is the main source of the debonding energy of G.

3.3. Effect of Water Content on the Debonding Properties of G

Due to the hydrophilicity of the G and C-S-H surfaces, invading water is easily fixed on the interlayer void between the G and C-S-H substrates. In order to clarify the influence of humidity on the interfacial bonding strength between G and C-S-H, four systems with different water contents were constructed, including a dry condition, one layer of water molecules, two layers of water molecules, and three layers of water molecules present on the interlayer void as shown in Figure 6. To ensure structural stability, we fixed the C-S-H substrate. We performed a tensile test after 1ns of relaxation of the system.

(**a**) Dry   (**b**) One layer

(**c**) Two layers   (**d**) Three layers
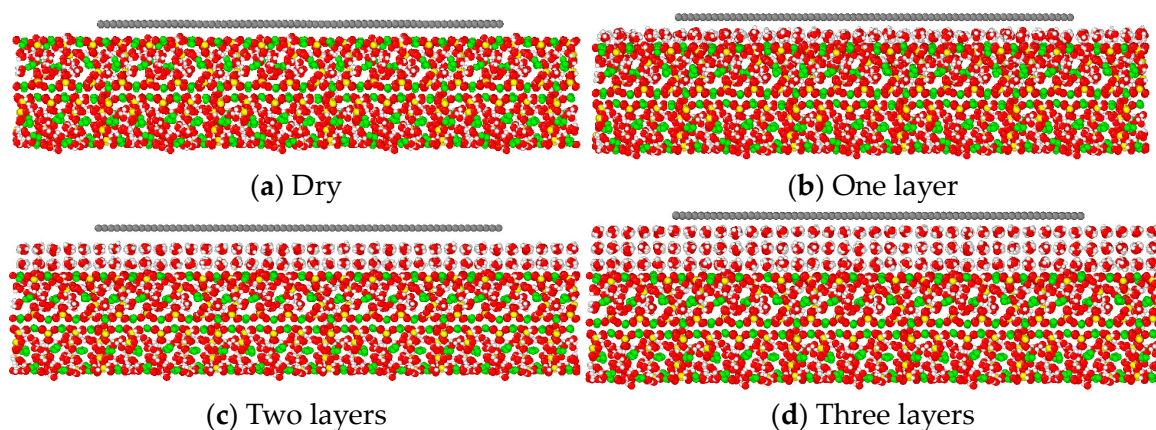
Figure 6. Initial structure of (**a**) a dry condition model, (**b**) one-layer water molecular model, (**c**) two-layers water molecular model, and (**d**) three-layers water molecular model. Graphene is gray, which is on a C-S-H substrate.

Figure 7 shows the time evolution of debonding tension F and the debonding tension work W of G under different water contents. The results show that the tension first increases and then decreases with an increase in time, and the work gradually increases with an increase in time and finally tends to a constant value. The tensile force of G debonding under the Dry and One-layer models reached the maximum value at about 5000 ps, which was 1.42×10^3 pN and 1.32×10^3 pN respectively, while the tensile force of G debonding under the Two-layers and Three-layers models reached the maximum value at about 5500 ps. They were 0.96×10^3 pN and 0.94×10^3 pN, respectively. At 10,000 ps, G is almost completely unbonded on the C-S-H substrate, and the limiting effect of C-S-H on the graphene fails, so the tension tends to zero and the work tends to a fixed value, which is the final work W_{max}.
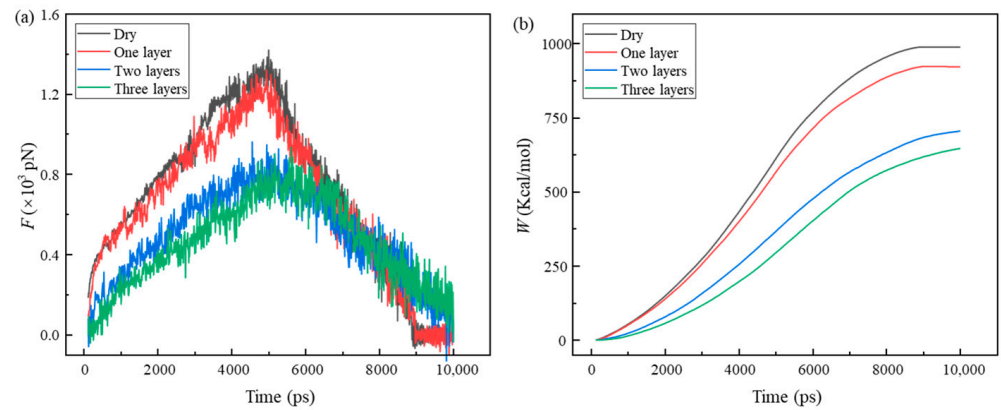
Figure 7. (**a**) Change of *F* with time and (**b**) change of *W* with time under different water contents.

Figure 8 shows the maximum pulling force F_{max} and the final work W_{max} generated by G debonding on a C-S-H substrate at different water contents. In general, both Fmax and W_{max} decreased with an increase in water content. When the interface is Dry (Dry), G is in close contact with C-S-H, and the binding between the two is all due to the van der Waals force between C-S-H and G. When a small amount of water intrudes into the interface (One layer), water forms hydrogen bonds with the surface of C-S-H, which is specifically manifested as the formation of a water film attached to the surface of C-S-H, slightly weakening the binding effect between G and C-S-H, and slightly reducing Fmax and W_{max}. When a large amount of water intrudes into the interface (water layer ≥ two), the water molecules attached to the surface of C-S-H play a lubricating role in isolating C-S-H and G, reducing the binding effect between the two, and significantly reducing F_{max} and W_{max}. As the water content continues to increase, the binding effect between G and C-S-H tends to be zero, that is, G loses its strengthening effect.
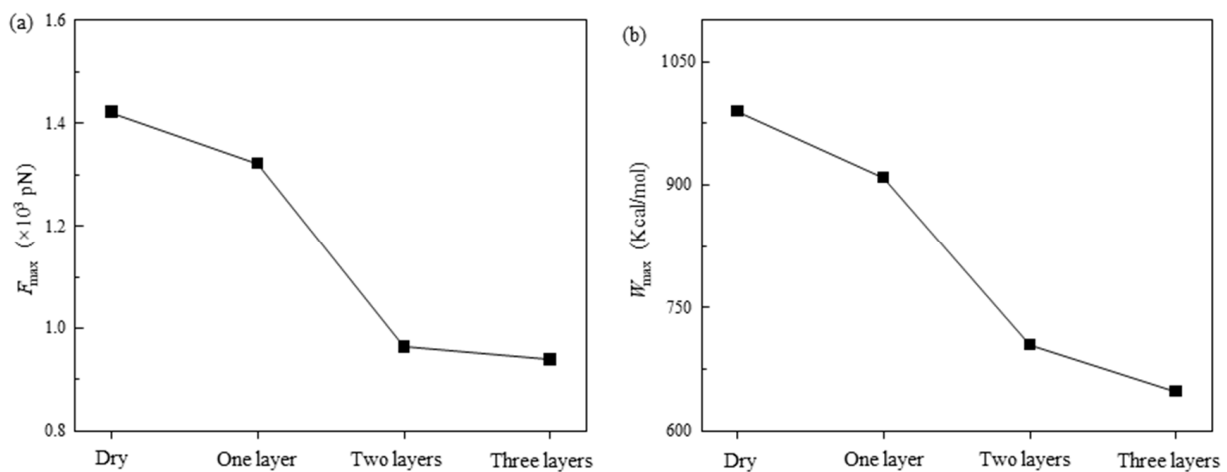
Figure 8. (**a**) F_{max} and (**b**) W_{max} at different water contents.

3.4. Analysis of the Adhesion Mechanism Between the G/C-S-H Interface

The F_{max} and W_{max} in dry environments are higher than those in humid environments (as shown in Figure 8). At high relative humidity, the material surface adsorbs moisture, and the adhesion may decrease due to the formation of a water film. In the case of low relative humidity, the surface of the material loses moisture, and the adhesion force may increase due to the increase in direct contact area.

It is worth noting that the mechanisms of adhesion and debonding behavior vary significantly depending on the materials involved. Adhesion primarily arises from intermolecular forces such as van der Waals forces and electrostatic interactions. These forces are influenced by the chemical composition and surface properties of the materials in contact.

For instance, polar materials tend to exhibit stronger electrostatic interactions due to their charged surface groups. Moreover, chemical bonding between the adhering surfaces can significantly enhance adhesion. This includes covalent bonding, hydrogen bonding, and ionic bonding, which are often stronger than intermolecular forces. The formation of these bonds depends on the reactivity of the surface groups and the conditions under which they interact. Additionally, mechanical interlocking can contribute to adhesion, particularly when one of the materials has a porous or rough surface. The adhesive can penetrate these irregularities, creating a physical lock that increases adhesion strength. Detachment or debonding occurs when the forces holding the adhering surfaces together are overcome. This can happen through interfacial failure, where the bond between the adhesive and the substrate weakens, or through cohesive failure, where the material itself breaks apart. The detachment mechanism is influenced by the material's mechanical properties, such as tensile strength and ductility. Materials with high tensile strength and ductility are more resistant to cohesive failure, whereas materials with weak interfacial bonds are more prone to interfacial failure.

In a dry environment, the molecular distance between the G and C-S-H interface is relatively close, so the van der Waals force (i.e., intermolecular attraction) is relatively strong. This force is one of the main sources of adhesion between the G and C-S-H interface. In humid environments, due to the presence of water molecules, the molecular distance between the G and C-S-H interface is increased, and the van der Waals force is weakened, resulting in a decrease in adhesion performance. In some cases, G or C-S-H surfaces may contain oxygen-containing functional groups, which may form hydrogen bonds between them. In a dry environment, the formation of hydrogen bonds helps to enhance adhesion performance between the G and C-S-H interface. However, in humid environments, water molecules may form hydrogen bonds with these oxygen-containing functional groups, weakening hydrogen bonding between G and C-S-H, resulting in reduced adhesion performance. Permeation of water molecules may cause minor changes in the structure of C-S-H, such as expansion or softening. This is similar to previous results. In work related to asphalt research, an appropriate amount of water can enhance adhesion of the interface, but a high water content may cause water molecules to overflow from foam asphalt and combine with aggregates, which will reduce adhesion of the interface [39].

These changes may alter the chemical and physical properties of the C-S-H surface, thereby affecting its adhesion performance with G. Meanwhile, G may undergo minor structural changes such as lattice distortion or surface reconstruction in humid environments, which may also affect its adhesion performance with C-S-H. Research findings from molecular dynamics simulations concerning interfacial humidity hold significant implications for guiding experimental endeavors. These simulations provide an atomic-level understanding of how water molecules interact with various surfaces, influencing factors such as wettability, adhesion, and the stability of interfaces. Guided by these predictions, experimental setups can be designed to test the durability of materials under controlled humidity conditions, helping to identify and mitigate potential failure mechanisms. And understanding how humidity affects the molecular structure and dynamics of the G/C-S-H interface can guide the synthesis of materials with enhanced stability or responsiveness to moisture. Experimental verification of these novel materials then ensures their practical applicability. By bridging the gap between atomic-scale simulations and macroscopic experimental observations, these findings provide a robust framework for designing, testing, and optimizing materials and systems that operate effectively in humid environments.

4. Conclusions

In this paper, the debonding behavior of G (graphene) on a C-S-H (calcium silicate hydrate) matrix was studied by a molecular dynamics method. The maximum tensile force (F_{max}) and maximum peeling work (W_{max}) obtained through molecular dynamics simulation analysis can be used as important indicators to evaluate the interfacial bonding strength between G and C-S-H. These values can effectively characterize the difficulty of

peeling under external forces and the required external energy. The following conclusions are drawn:

1. Under dry conditions, adhesion strength at the interface between G and C-S-H is strong, mainly influenced by van der Waals forces and possible hydrogen bonding interactions; in humid environments, an increase in moisture will weaken these interactions, leading to a decrease in adhesion performance.
2. As the number of interfacial water layers increases, the required tensile force and delamination work for the delamination of G at the C-S-H interface gradually decrease. Especially when the water layer exceeds two layers, water acts as a lubricant, significantly reducing interfacial adhesion performance.
3. The adhesion between G and C-S-H interfaces mainly originates from van der Waals forces rather than strong chemical bonding interactions. The presence of water weakens this interaction, resulting in a decrease in interfacial bonding strength.

By simulating and analyzing the behavior of G and C-S-H interfaces under different humidity conditions, this article provides theoretical guidance for experiments. This type of atomic scale simulation can help optimize the design of materials in humid environments, improving their durability and stability in practical applications.

Author Contributions: Y.H. acquired the grant and revised the paper; Y.H. and Y.Z. performed modeling and wrote the paper; Y.H. and Y.W. extracted and analyzed the data; T.C. checked the grammar. All authors have read and agreed to the published version of the manuscript.

Institutional Review Board Statement: Not applicable.

Informed Consent Statement: Not applicable.

Data Availability Statement: Data are contained within the article.

Conflicts of Interest: Author Yongliang Han, was employed by the company CCTEG Xian Research Institut (Group) Co., Ltd., authors Yongliang Han, Yongzhe Zhao and Yijie Wang were employed by the company CCTEG Xi'an Geothermal Energy Development Co., Ltd. The remaining authors declare that the research was conducted in the absence of any commercial or financial relationships that could be construed as a potential conflict of interest.

References

1. Geim, A.K. Graphene: Status and prospects. *Science* **2009**, *324*, 1530–1534. [CrossRef] [PubMed]
2. Banhart, F.; Kotakoski, J.; Krasheninnikov, A.V. Structural defects in graphene. *ACS Nano* **2011**, *5*, 26–41. [CrossRef] [PubMed]
3. Balandin, A.A.; Ghosh, S.; Bao, W.; Calizo, I.; Teweldebrhan, D.; Miao, F.; Lau, C.N. Superior thermal conductivity of single-layer graphene. *Nano Lett.* **2008**, *8*, 902–907. [CrossRef] [PubMed]
4. Yang, Y.; Cao, J.; Wei, N.; Meng, D.; Wang, L.; Ren, G.; Yan, R.; Zhang, N. Thermal conductivity of defective graphene oxide: A molecular dynamic study. *Molecules* **2019**, *24*, 1103. [CrossRef]
5. Chen, D.; Feng, H.; Li, J. Graphene oxide: Preparation, functionalization, and electrochemical applications. *Chem. Rev.* **2012**, *112*, 6027–6053. [CrossRef]
6. Kai, M.; Zhang, L.; Liew, K. Graphene and graphene oxide in calcium silicate hydrates: Chemical reactions, mechanical behavior and interfacial sliding. *Carbon* **2019**, *146*, 181–193. [CrossRef]
7. Dai, Z.; Lu, N.; Liechti, K.M.; Huang, R. Mechanics at the interfaces of 2D materials: Challenges and opportunities. *Curr. Opin. Solid State Mater. Sci.* **2020**, *24*, 100837. [CrossRef]
8. Ghazizadeh, S.; Duffour, P.; Skipper, N.; Billing, M.; Bai, Y. An investigation into the colloidal stability of graphene oxide nano-layers in alite paste. *Cem. Concr. Res.* **2017**, *99*, 116–128. [CrossRef]
9. Lin, W.; Zhang, C.; Fu, J.; Xin, H. Dynamic mechanical behaviors of calcium silicate hydrate under shock compression loading using molecular dynamics simulation. *J. Non-Cryst. Solids* **2018**, *500*, 482–486. [CrossRef]
10. Fan, D.; Lue, L.; Yang, S. Molecular dynamics study of interfacial stress transfer in graphene-oxide cementitious composites. *Comput. Mater. Sci.* **2017**, *139*, 56–64. [CrossRef]

11. Zhao, L.; Guo, X.; Song, L.; Song, Y.; Dai, G.; Liu, J. An intensive review on the role of graphene oxide in cement-based materials. *Constr. Build. Mater.* **2020**, *241*, 117939. [CrossRef]

12. Yang, Y.; Cao, J.; Wu, P.; Luo, T.; Liang, T.; Yin, H.; Yuan, K. Effect of temperature on interface debonding behavior of graphene/graphene-oxide on cement-based composites. *Surf. Interfaces* **2024**, *47*, 104198. [CrossRef]

13. Mukherjee, K.; Rajender, A.; Samanta, A.K. A review on the fresh properties, mechanical and durability performance of graphene-based cement composites. *Mater. Today Proc.* **2023**, *in press*.

14. Hou, D.; Zhang, W.; Chen, Z.; Zheng, Q.; Sun, G.; Liang, R. A molecular dynamics study of silicene reinforced cement composite at different humidity: Surface structure, bonding, and mechanical properties. *Constr. Build. Mater.* **2021**, *291*, 123242. [CrossRef]

15. Fan, L.; Song, F.; Xu, J.; Wang, H.; Wang, F. Interlayer sp3 Bonds and Chirality at Bilayer Graphene Oxide/Calcium Silicate Hydrate Abnormally Enhance Its Interlayer Stress Transfer. *ACS Omega* **2024**, *9*, 10343–10352. [CrossRef] [PubMed]

16. Miao, X.; Xing, Y.; Zheng, H.; Liu, Q.; Hu, M.; Guo, J. Effects of hybrid graphene oxide-nanosilica on calcium silicate hydrate in the simulation environment and cement. *ACS Omega* **2023**, *8*, 22975–22983. [CrossRef]

17. Liang, T.; Lai, Y.; Hou, D.; Pei, W.; Wang, M.; Yu, F.; Yang, Q.; Yang, Y.; Li, H. Molecular dynamics simulation investigation on the anti-freezing mechanisms of CSH-GS/GO interfaces. *Constr. Build. Mater.* **2023**, *369*, 130581. [CrossRef]

18. Aadithya, M.; Sunil, R.; Gomosta, S.; Maliyekkal, S.M.; Rahul, A. Behavior of functionalized graphene in fresh and hydrated cement matrix: Role of carboxyl and amine functional group. *Constr. Build. Mater.* **2024**, *450*, 138542. [CrossRef]

19. Lu, L.; Zhang, Y.; Yin, B. Structure evolution of the interface between graphene oxide-reinforced calcium silicate hydrate gel particles exposed to high temperature. *Comput. Mater. Sci.* **2020**, *173*, 109440. [CrossRef]

20. Gronchi, P.; Bianchi, S.; Brambilla, L.; Goisis, M. Graphite Nanoplatelets and Graphene Oxide Influence on CSH Formation. In *Superplasticizers and Other Chemical Admixtures in Concrete*; ACI-American Concrete Institute: Farmington Hills, MI, USA, 2018; pp. 237–256.

21. Hou, D.; Lu, Z.; Li, X.; Ma, H.; Li, Z. Reactive molecular dynamics and experimental study of graphene-cement composites: Structure, dynamics and reinforcement mechanisms. *Carbon* **2017**, *115*, 188–208. [CrossRef]

22. Chen, W.; Lu, S.; Yu, S.; Gong, C.; Wang, Z.; Gao, Y. Effects of graphene oxide on shearing performance of C–S–H composites: A molecular dynamics study. *J. Mater. Sci.* **2023**, *58*, 16972–16987. [CrossRef]

23. Long, Z.; You, L.; Tang, X.; Ma, W.; Ding, Y.; Xu, F. Analysis of interfacial adhesion properties of nano-silica modified asphalt mixtures using molecular dynamics simulation. *Constr. Build. Mater.* **2020**, *255*, 119354. [CrossRef]

24. Tam, L.-h.; He, L.; Wu, C. Molecular dynamics study on the effect of salt environment on interfacial structure, stress, and adhesion of carbon fiber/epoxy interface. *Compos. Interfaces* **2019**, *26*, 431–447. [CrossRef]

25. Lyu, Y.; Huang, Q.; Liu, L.; Zhang, D.; Xue, H.; Zhang, F.; Zhang, H.; Li, R.; Wang, Q. Experimental and molecular dynamics simulation investigations of adhesion in heavy oil/water/pipeline wall systems during cold transportation. *Energy* **2022**, *250*, 123811. [CrossRef]

26. Ranathunga, D.T.; Shamir, A.; Dai, X.; Nielsen, S.O. Molecular dynamics simulations of water condensation on surfaces with tunable wettability. *Langmuir* **2020**, *36*, 7383–7391. [CrossRef]

27. Büyüköztürk, O.; Buehler, M.J.; Lau, D.; Tuakta, C. Structural solution using molecular dynamics: Fundamentals and a case study of epoxy-silica interface. *Int. J. Solids Struct.* **2011**, *48*, 2131–2140. [CrossRef]

28. Yang, Y.; Cao, J. New insight on the interfacial behavior between graphene-based membranes and protonated silicon-dioxide via molecular dynamics simulations. *Appl. Surf. Sci.* **2022**, *590*, 152727. [CrossRef]

29. Pellenq, R.J.-M.; Kushima, A.; Shahsavari, R.; Van Vliet, K.J.; Buehler, M.J.; Yip, S.; Ulm, F.-J. A realistic molecular model of cement hydrates. *Proc. Natl. Acad. Sci. USA* **2009**, *106*, 16102–16107. [CrossRef] [PubMed]

30. Hou, D.; Yang, Q.; Jin, Z.; Wang, P.; Wang, M.; Wang, X.; Zhang, Y. Enhancing interfacial bonding between epoxy and CSH using graphene oxide: An atomistic investigation. *Appl. Surf. Sci.* **2021**, *568*, 150896. [CrossRef]

31. Cygan, R.T.; Liang, J.-J.; Kalinichev, A.G. Molecular models of hydroxide, oxyhydroxide, and clay phases and the development of a general force field. *J. Phys. Chem. B* **2004**, *108*, 1255–1266. [CrossRef]

32. Watkins, E.K.; Jorgensen, W.L. Perfluoroalkanes: Conformational analysis and liquid-state properties from ab initio and Monte Carlo calculations. *J. Phys. Chem. A* **2001**, *105*, 4118–4125. [CrossRef]

33. Yang, Y.; Wang, Y.; Cao, J. Prediction and evaluation of thermal conductivity in nanomaterial-reinforced cementitious composites. *Cem. Concr. Res.* **2023**, *172*, 107240. [CrossRef]

34. Mishra, R.K.; Mohamed, A.K.; Geissbühler, D.; Manzano, H.; Jamil, T.; Shahsavari, R.; Kalinichev, A.G.; Galmarini, S.; Tao, L.; Heinz, H. cemff: A force field database for cementitious materials including validations, applications and opportunities. *Cem. Concr. Res.* **2017**, *102*, 68–89. [CrossRef]

35. Liang, T.; Lai, Y.; Hou, D.; Yang, Q.; Yang, Y.; Bai, R.; Zhang, J.; Jiang, J. Freezing mechanism of NaCl solution ultra-confined on surface of calcium-silicate-hydrate: A molecular dynamics study. *Cem. Concr. Res.* **2022**, *154*, 106722. [CrossRef]

36. Hou, D.; Zheng, H.; Wang, P.; Wan, X.; Wang, M.; Wang, H. Molecular insight in the wetting behavior of nanoscale water droplet on CSH surface: Effects of Ca/Si ratio. *Appl. Surf. Sci.* **2022**, *587*, 152811. [CrossRef]

37. Thompson, A.P.; Aktulga, H.M.; Berger, R.; Bolintineanu, D.S.; Brown, W.M.; Crozier, P.S.; In 't Veld, P.J.; Kohlmeyer, A.; Moore, S.G.; Nguyen, T.D. LAMMPS-a flexible simulation tool for particle-based materials modeling at the atomic, meso, and continuum scales. *Comput. Phys. Commun.* **2022**, *271*, 108171. [CrossRef]

38. Park, S.; Khalili-Araghi, F.; Tajkhorshid, E.; Schulten, K. Free energy calculation from steered molecular dynamics simulations using Jarzynski's equality. *J. Chem. Phys.* **2003**, *119*, 3559–3566. [CrossRef]
39. Rose, S.; Prevoteau, A.; Elzière, P.; Hourdet, D.; Marcellan, A.; Leibler, L. Nanoparticle solutions as adhesives for gels and biological tissues. *Nature* **2014**, *505*, 382–385. [CrossRef]